Exploration of New Concepts for Mass Detection in Electrostatically-Actuated Structures Based on Nonlinear Phenomena

Mohammad I. Younis
e-mail: myounis@binghamton.edu

Fadi Alsaleem

Department of Mechanical Engineering,
State University of New York at Binghamton,
Binghamton, NY 13902

This study presents an effort to explore the exploitation of dynamic instabilities and bifurcations in micro-electro-mechanical systems to realize novel methods and functionalities for mass sensing and detection. These instabilities are induced by exciting a microstructure with a nonlinear forcing composed of a dc parallel-plate electrostatic load and an ac harmonic load. The frequency of the ac load is tuned to be near the fundamental natural frequency of the structure (primary resonance) or its multiples (subharmonic resonance). For each excitation method, local bifurcations, such as saddle-node and pitchfork, and global bifurcations, such as the escape phenomenon, may occur. This work aims to explore the utilization of these bifurcations to design novel mass sensors and switches of improved characteristics. One explored concept of a device is a switch triggered by mass threshold. The basic idea of this device is based on the phenomenon of escape from a potential well. This device has the potential of serving as a smart switch that combines the functions of two devices: a sensitive gas/mass sensor and an electromechanical switch. The switch can send a strong electrical signal as a sign of mass detection, which can be used to actuate an alarming system or to activate a defensive or a security system. A second type of explored devices is a mass sensor of amplified response. The basic principle of this device is based on the jump phenomena encountered in pitchfork bifurcations during mass detection. This leads to an amplified response of the excited structure making the sensor more sensitive and its signal easier to be measured. As case studies, these device concepts are first demonstrated by simulations on clamped-clamped and cantilever microbeams. Results are presented using long-time integration for the equations of motion of a reduced-order model. An experimental case study of a capacitive sensor is presented illustrating the proposed concepts. It is concluded that exciting a microstructure at twice its fundamental natural frequency produces the most promising results for mass sensing and detection. [DOI: 10.1115/1.3079785]

Keywords: MEMS, electrostatic force, dynamic pull-in, mass and gas sensors, switches, escape phenomenon

1 Introduction

There has been extensive research in recent years in the field of mass sensing and detection. This is driven primarily by the increasing demand to push the limits of mass sensing to enable reliable and precise detection of extremely small masses, such as those of viruses and DNA molecules. Also, this has been boosted by the need to detect very low gas concentration for gas sensing applications. In addition, lowering the cost of mass sensors and achieving smart and multifunctionality on a single chip have been major driving forces. This study presents an attempt to explore alternative methods to achieve some of these goals by utilizing the complexity in the dynamics of electrostatically-actuated micro-electro-mechanical systems (MEMS). The focus of this research, in particular, is on resonant microsensors employing microbeams.

1.1 Microbeam-Based Mass Sensors. Many mass sensors rely on a microbeam, mostly a cantilever, which is coated with a sorbent material that is sensitive to a specific substance (analyte) [1–36]. The coated material absorbs the analyte, such as a gas or a biological molecule. The analyte increases the mass of the cantilever beam and it may induce bending stress on the surface of the beam causing its deflection. The deflection can be measured using an optical-readout system, for example, and then it is related to the mass of the analyte. This method is called static sensing mode [4]. This mode does not provide high sensitivity of detection since the deflection is usually very small compared with the length of the beam. Sensitivity of detection is crucial for many chemical [1–9] and biological [10–15] applications, such as to detect small gas concentration emitted from explosive material or to detect small viruses and bacteria. One way to improve sensitivity is through dynamic mode of sensing. Here, the beam is driven at resonance. When it absorbs an analyte, its mass increases, and hence its natural frequency decreases. This shift in frequency can be tracked, measured, and related to the mass of the analyte. Although the amplitude of beam oscillation itself is not directly related to the detected mass, it is desirable to have it as large as possible (high quality factor). This facilitates tracking and measuring the resonance peak. The sharper the resonance peak is, the more sensitive the mass sensor is considered. Increasing the quality factor can be achieved by placing the microbeam in reduced

Contributed by the Design Engineering Division of ASME for publication in the JOURNAL OF COMPUTATIONAL AND NONLINEAR DYNAMICS. Manuscript received January 8, 2008; final manuscript received July 9, 2008; published online March 10, 2009. Review conducted by Albert C. J. Luo.

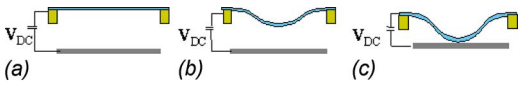

Fig. 1 Schematic showing the parallel-plate dc electrostatic actuation and the pull-in instability (*a*) $V_{DC}=0$, (*b*) below pull in, (*c*) pull-in

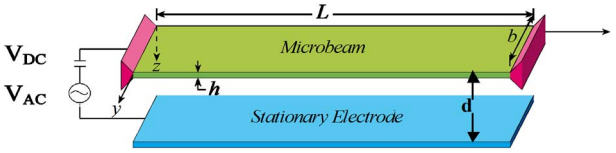

Fig. 3 A MEMS parallel-plate capacitor showing a dynamic ac+dc actuation

pressure environment. However, mass sensors usually are desirable to operate in air at atmospheric pressure to capture the analyte of interest. In some applications, it is even desirable to operate in fluids such as blood. Therefore, controlling the quality factor or damping may not be achievable or adequate in itself.

Other methods to increase sensitivity have been explored to enable the detection of very small substances and lower gas concentration. One approach is through miniaturizing the microbeam to submicro and nanoscales [16–23]. However, one shortcoming of miniaturization is that the coated surface of the beam shrinks and becomes too small. This may make the coated surface less reliable transducer from a chemical or biological perspective. Other issues, such as the noise level, repeatability of measurements, and reliability issues, become of increasing concerns. Several dynamical methods have been explored to enhance sensitivity, such as higher-order-mode excitations [24–28], parametric excitation [32–34], beam coupling [10,35], and feedback control amplification [36]. This work aims to explore new methods to increase mass sensitivity and achieve new functionality through utilizing the principles of dynamics instabilities in electrostatic MEMS.

1.2 Electrostatic Actuation and Dynamic Pull-In. Parallel-plate electrostatic force is a common actuation method in MEMS (Fig. 1). It depends in a nonlinear way on the separation between two electrodes. In this method, a movable structure (upper electrode) is biased by an electrostatic load V_{dc} and is mounted above a stationary lower electrode. A dc force deflects the structure toward the stationary electrode. If V_{dc} is small, the structure stays in the deflected position, at which the elastic restoring force of the structure is in equilibrium with the opposing electrostatic force (Fig. 1(*b*)). There is an upper limit for V_{dc}, beyond which the mechanical restoring force of the structure can no longer resist the opposing electrostatic force. This leads to a sudden collapse of the structure, which hits the stationary electrode (Fig. 1(*c*)). This structural instability phenomenon is known as pull-in and the associated voltage is called pull-in voltage [37]. Figure 2 illustrates the pull-in instability from an energy perception. Figure 2(*a*) indicates that below pull-in, a biased structure undergoes free stable oscillation when perturbed from its equilibrium position (see the closed loops in the phase portrait). However, if it is given enough high initial velocity, the structure may collapse, as indicated from the open-loop trajectory in the phase portrait of Fig. 2(*a*). In other words, it will escape from the electrostatic potential well. This phenomenon is known as dynamic pull-in. Pull-in is undesirable for most MEMS sensors. However, MEMS switches [38] utilize pull-in to actuate a structure in a large stroke and short time.

Another form of actuation utilizes a dc load superimposed on an ac harmonic load, Fig. 3, of amplitude V_{ac} and frequency Ω. Here, V_{dc} deflects slightly the movable electrode and V_{ac} vibrates the electrode around the new deflected position. Resonant sensors, including some mass sensors, rely on this actuation method. Dynamic pull-in also occurs here, which is caused by a dynamic (harmonic) load. Dynamic pull-in in this case is triggered at much lower voltage compared with the static case. In previous works [39,40], dynamic pull-in instability has been investigated for a clamped-clamped microbeam excited near its fundamental natural frequency (primary resonance) and half (superharmonic) and twice (subharmonic) the fundamental natural frequency (secondary resonances). Those studies revealed several mechanisms and routes to dynamic pull-in including homoclinic tangling, saddle-node bifurcation, period-doubling bifurcation, and the escape phenomenon. Next, we will explain how to utilize some of those to realize new mass sensor ideas. Also, we will explore the device opportunities and potential in cantilever microbeams based on their distinctive dynamical behavior.

2 Primary Resonance of Clamped-Clamped Beams

2.1 Modeling and Simulation Methodology. We start this study by analyzing the response of clamped-clamped microbeams to ac+dc actuation, Fig. 3. The equation of motion governing the transverse deflection $w(x,t)$ of the microbeam is expressed as

$$EI\frac{\partial^4 w}{\partial x^4}+\rho bh\frac{\partial^2 w}{\partial t^2}+\tilde{c}\frac{\partial w}{\partial t}=\left[\frac{Ebh}{2L}\int_0^L\left(\frac{\partial w}{\partial x}\right)^2 dx+\tilde{N}\right]\frac{\partial^2 w}{\partial x^2}+\frac{\varepsilon b[V_{dc}+V_{ac}\cos(\Omega t)]^2}{2(d-w)^2} \quad (1)$$

where x is the position along the microbeam length, I is the moment of inertia of the cross section, E is Young's modulus, t is time, ρ is the material density, h and b are the microbeam thickness and width, d is the gap width, and ε is the dielectric constant of the gap medium. The parameter $\tilde{N}$ corresponds to a tensile or compressive axial load, depending on whether it is positive or negative. The integral term in Eq. (1) represents the midplane stretching of the microbeam in the case of immovable boundary

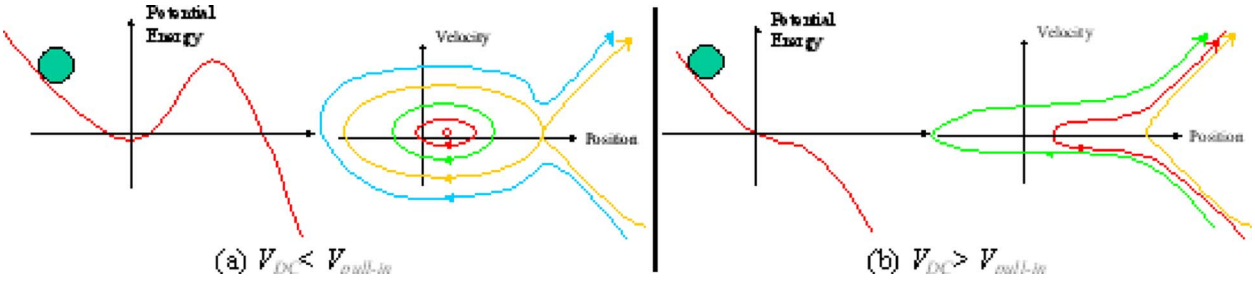

Fig. 2 The total potential energy (electrostatic+stiffness) and the corresponding phase portrait for a parallel-plate capacitor for the case of a voltage load below pull-in (*a*) and above pull-in (*b*)

conditions. For the case of cantilever microbeams, this term is set equal to zero. The microbeam is subject to a viscous damping, which can be due to squeeze-film damping. We assume this effect to be negligible and assume a constant damping coefficient $\tilde{c}$ per unit length.

For convenience, we introduce the nondimensional variables (denoted by hats)

$$\hat{x} = \frac{x}{L}, \quad \hat{t} = \frac{t}{\tilde{t}}, \quad \hat{w} = \frac{w}{d} \tag{2}$$

where $\tilde{t}$ is a time scale, defined below. Substituting Eq. (2) into Eq. (1) and dropping the hats, we obtain

$$\frac{\partial^4 w}{\partial x^4} + \frac{\partial^2 w}{\partial t^2} + c\frac{\partial w}{\partial t} = \left[\alpha_1 \int_0^1 \left(\frac{\partial w}{\partial x}\right)^2 dx + N\right]\frac{\partial^2 w}{\partial x^2} + \frac{\alpha_2[V_{\mathrm{dc}} + V_{\mathrm{ac}}\cos(\Omega t)]^2}{(1-w)^2} \tag{3}$$

The nondimensional parameters appearing in Eq. (3) are

$$\alpha_1 = 6\left(\frac{d}{h}\right)^2, \quad \alpha_2 = \frac{6\varepsilon L^4}{Eh^3 d^3}, \quad c = \frac{12\hat{c}L^4}{ETbh^3}, \quad N = \frac{12\tilde{N}L^2}{Ebh^3}$$
$$\tilde{t} = \sqrt{\frac{\rho bhL^4}{EI}} \tag{4}$$

Next, we generate a reduced-order model by discretizing Eq. (3) into a finite-degree-of-freedom system consisting of ordinary-differential equations in time. The undamped linear mode shapes of the straight (unactuated) microbeam may be used as basis functions in the Galerkin procedure. To this end, we express the deflection as

$$w(x,t) = \sum_{i=1}^{M} u_i(t)\phi_i(x) \tag{5}$$

where $u_i(t)$ is the ith generalized coordinate and $\phi_i(x)$ is the ith linear undamped mode shape of the straight microbeam. Multiplying Eq. (3) by $\phi_i(x)\,(1-w)^2$, substituting Eq. (5) into the resulting equation, and integrating the outcome from $x=0$ to 1 yields the following reduced-order model:

$$\begin{aligned}
&\ddot{u}_n - 2\sum_{i,j=1}^{M}\Lambda_{ijn}u_j\ddot{u}_i + \sum_{i,j,k=1}^{M}\Lambda_{ijkn}u_k u_j\ddot{u}_i - c\dot{u}_n - \omega_n^2 u_n \\
&= \alpha_2\Lambda_n[V_{\mathrm{dc}} + V_{\mathrm{ac}}\cos(\Omega t)]^2 + 2\sum_{i,j=1}^{M}\omega_i^2\Lambda_{ijn}u_j u_i \\
&\quad - \sum_{i,j,k=1}^{M}\omega_i^2\Lambda_{ijkn}u_k u_j u_i + 2c\sum_{i,j=1}^{M}\Lambda_{ijn}u_j\dot{u}_i - c\sum_{i,j,k=1}^{M}\Lambda_{ijkn}u_k u_j\dot{u}_i \\
&\quad + \alpha_1\sum_{i,j,k=1}^{M}u_k u_j u_i\Gamma(\phi_i,\phi_j)\int_0^1\phi_n\phi_k''dx \\
&\quad - 2\alpha_1\sum_{i,j,k,l=1}^{M}u_k u_j u_i u_l\Gamma(\phi_i,\phi_j)\int_0^1\phi_n\phi_k\phi_l''dx \\
&\quad + \alpha_1\sum_{i,j,k,l,m=1}^{M}u_i u_j u_k u_l u_m\Gamma(\phi_i,\phi_j)\int_0^1\phi_l\phi_m\phi_n\phi_k''dx
\end{aligned} \tag{6}$$

where the prime denotes differentiation with respect to space x, the overdot denotes differentiation with respect to the time t, ω_i is the ith natural frequency of the microbeam, and the functionals Λ and Γ are defined as

$$\Lambda_n = \int_0^1\phi_n dx, \quad \Lambda_{in} = \int_0^1\phi_i\phi_n dx, \quad \Lambda_{ijn} = \int_0^1\phi_i\phi_j\phi_n dx, \ldots \tag{7}$$

$$\Gamma(f,g) = \int_0^1\frac{\partial f}{\partial x}\frac{\partial g}{\partial x}dx \tag{8}$$

In previous works [41,42], we found that using three symmetric mode shapes in the reduced-order model leads to converged results for the stable response of clamped-clamped microbeams. In Refs. [39,40], the reduced-order model was implemented in a shooting technique to find periodic motions and their stability for clamped-clamped microbeams. Here, we apply direct-time integration on the reduced-order model equations, using three mode shapes, over sufficiently long period of time until a steady-state stable solution is found. Direct time integration is implemented using an explicit Runge–Kutta method using a built-in routine in the software MATHEMATICA [43]. As will be shown below, both direct-time integration and the shooting technique yield close results for the stable response. Direct integration, however, does not capture unstable solutions and suffer some convergence problems near bifurcation points. However, since the focus of this paper is to draw the attention to the potential of the nonlinear dynamics of electrostatic MEMS more than investigating bifurcations, long-time integration will be used since it serves well this purpose.

2.2 Switch Triggered by Mass Detection STMT. Next, we show simulation results on a microbeam, which was simulated previously in previous works [39,40] using a shooting technique to enable comparisons with the long-time integration results. The microbeam has a length $L=510\ \mu$m, thickness $h=1.5\ \mu$m, width $b=100\ \mu$m, and a gap width separating the microbeam from the substrate $d=1.18\ \mu$m. The microbeam is biased by $V_{\mathrm{ac}}=2$ V and placed in a reduced pressure with a quality factor equal 1000. The microbeam is subjected to a tensile axial stress such that $\tilde{N}=0.159$ mN. The pull-in voltage for the microbeam due to dc voltage only is $V_{\mathrm{dc}}=4.8$ V. The natural frequency of the microbeam is $\omega_{\mathrm{natural}}=23.9\omega_{\mathrm{universal}}$, where $\omega_{\mathrm{universal}}$ is a universal characteristic frequency for a microbeam of any boundary conditions [44,45]. It is expressed as $\omega_{\mathrm{universal}}=\sqrt{Ebh^3/12mL^3}$, where m is the mass of the beam. Figure 4(*a*) shows that at $V_{\mathrm{ac}}=0.01$ V, the microbeam exhibits a nonlinear hardening behavior characterized by a frequency-response curve bending to the right, hysteresis, and coexistence of multiple states. When V_{ac} is increased further, for example, $V_{\mathrm{ac}}=0.1$ V, the frequency-response curve is terminated by dynamic pull-in, which is remarked by a slope of the frequency-response curve approaching infinity. As V_{ac} is increased more, a band of frequencies is born, in which the microbeam cannot have a state of steady-state oscillation, such as the case of $V_{\mathrm{ac}}=0.5$ V. In other words, the microbeam tends to escape from the potential well of the electrostatic force to pull-in. A similar escape band of frequency was found in Ref. [39] using a shooting technique. The escape phenomenon is further illustrated in Fig. 4(*b*). This phenomenon of escaping from a potential well is a universal phenomenon characterizing all nonlinear systems with a hilltop potential well [46,47], such as that of the electrostatic force depicted in Fig. 2. As noted from Fig. 4, the escape band requires high values of V_{ac} and is generated at frequency band surrounding resonance. More clarification on the escape phenomenon will be presented in Sec. 3.

Next, we explain the idea of one of the proposed concepts for mass detection. Toward this we refer back to Fig. 4(*b*). The figure shows that by tuning some parameters of the system, V_{ac}, V_{dc}, and damping, a frequency band is generated where an oscillator cannot have a stable state (escape phenomenon). This means that if a microbeam is excited by an ac load of a frequency in the escape band, it must go directly to pull-in. We propose to utilize this

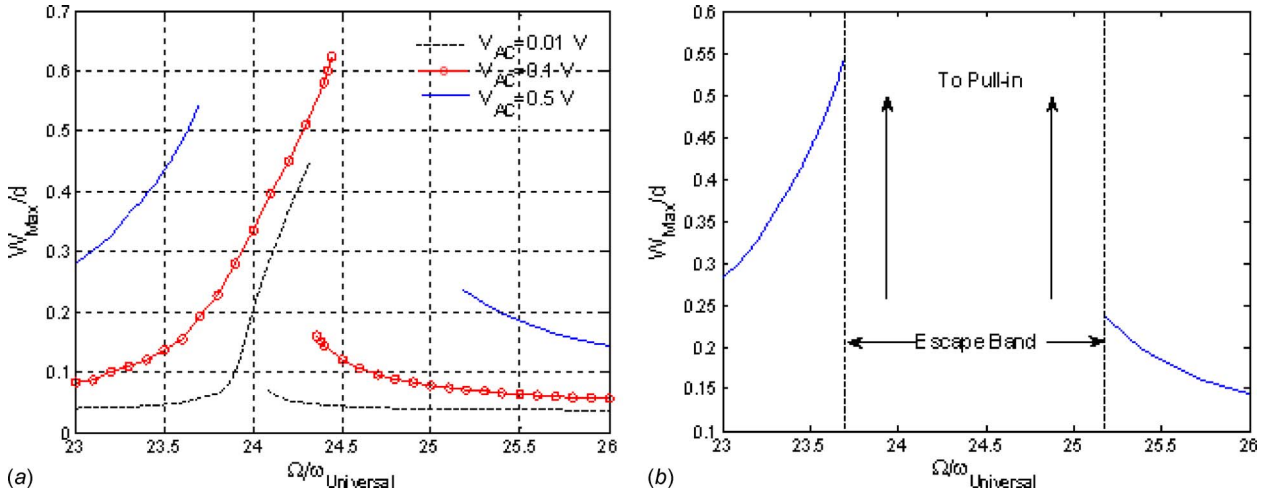

Fig. 4 (*a*) Frequency-response curves of a clamped-clamped microbeam excited near its first natural frequency for various values of ac loads. (*b*) For the case of V_{ac}=0.5 V showing the escape-to-pull-in frequency band.

phenomenon to design a smart switch triggered by mass threshold (STMT). In this concept, a microbeam, which is coated with a material sensitive to a specific analyte, is excited by a combination of a dc and ac harmonic load of a fixed frequency Ω below the escape band of frequencies, for example, at $\Omega/\omega_{\text{universal}}=23.5$ in Fig. 4(*b*). When the microbeam detects the existence of the specific substance desired to be detected, its mass m increases, $\omega_{\text{universal}}=\sqrt{Ebh^3/12mL^3}$ decreases, and hence the ratio $\Omega/\omega_{\text{universal}}$ increases and shifts to the right. The amount of frequency shift is proportional to the detected mass Δm. Assuming a uniform mass increase across the entire beam due to the analyte detection, the frequency shift can be calculated according to the below equation:

$$\frac{\left(\frac{\Omega}{\omega_{\text{universal}}}\right)_{\text{new}}}{\left(\frac{\Omega}{\omega_{\text{universal}}}\right)_{\text{old}}}=\frac{(\omega_{\text{universal}})_{\text{old}}}{(\omega_{\text{universal}})_{\text{new}}}=\sqrt{\frac{\frac{Ebh^3}{12L^3m}}{\frac{Ebh^3}{12L^3m_{\text{new}}}}}=\sqrt{\frac{m_{\text{new}}}{m}} \tag{9}$$

Substituting $m_{\text{new}}=m+\Delta m$ yields

$$\left(\frac{\Omega}{\omega_{\text{universal}}}\right)_{\text{new}}=\left(\frac{\Omega}{\omega_{\text{universal}}}\right)_{\text{old}}\sqrt{\frac{\Delta m}{m}+1} \tag{10}$$

The shift can be calibrated such that the new $\Omega/\omega_{\text{universal}}$ lies in the escape band of frequencies when detecting a certain amount of analyte above a specific mass threshold (this can be a concentration threshold for gases). Hence, the microbeam collapses to close an electric circuit to indicate the presence of the gas and at the same time sends an electrical signal, which can be used for alarming or any other useful function.

To make the description of this concept clearer, we illustrate the previous scenario in Fig. 4(*b*) using dimensional quantities and plots. Consider the case in which the microbeam is initially excited by a combination of a dc and ac harmonic load of a fixed frequency below the escape band, for example, at 52 kHz in Fig. 5. We assume a 5% increase in its mass because of external mass detection/absorption. This leads to a decrease in its natural frequency shifting it to the left. This means that the whole frequency-response curve of the microbeam shifts to the left too. By maintaining the frequency of excitation fixed at 52 kHz while the microbeam's natural frequency shifting to smaller values, and by calibrating this shift such that the operating frequency lies in the escape band after mass detection, the microbeam will be forced to pull-in. Hence, it acts as a switch to close an electric circuit and pass an electric signal. Figure 5 shows simulated time-history response for the microbeam for two states, before and after mass detection. Prior to mass detection, the microbeam oscillates at a steady-state amplitude of 0.4 μm. After mass detection, the microbeam undergoes unstable oscillation leading to its collapse after 0.25 ms.

The idea of the STMT can offer many attractive features, especially in applications where measuring the quantity of mass is not as important as doing an action upon its detection. The STMT combines the functions of two devices: a mass sensor and an electromechanical switch. The device can detect an analyte, such as an explosive gas, and then sends instantaneously a strong electric signal as a sign of this detection. This signal can be used to

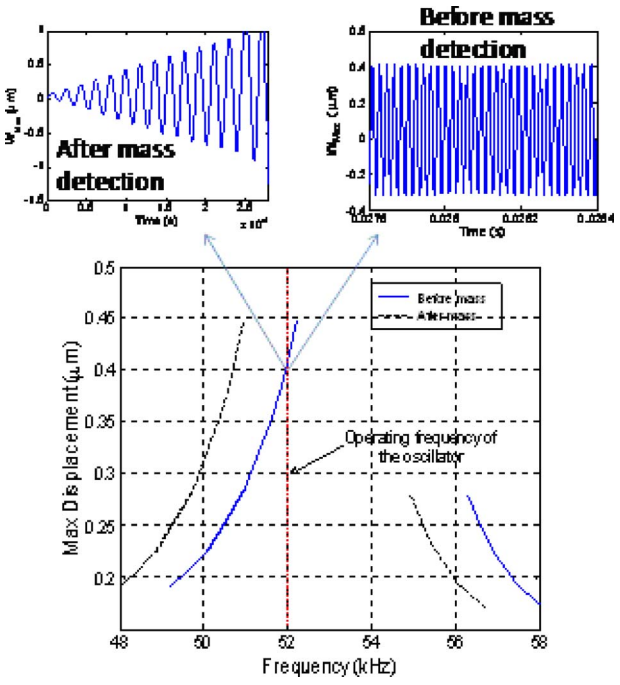

Fig. 5 Dimensional frequency-response curves for the clamped-clamped microbeam of Fig. 4(*b*) before and after 5% mass increase. Also shown are two time-history simulations for the response of the microbeam before and after mass detection when excited at a fixed frequency equal to 52 kHz.

actuate an alarming system or to activate a defensive or a security system. This new device concept is simple since it does not require complicated fabrication process. The complexity comes from the dynamics rather than fabrication. This can lower the cost of mass sensors for some applications where such functionality is desirable.

A vital characteristic of this concept is the sensitivity of detection and the smallest mass that can be detected to activate the switching action. This indicates that the frequency of excitation needs to be chosen just before the escape band of frequencies. The amplitude of vibration at such point, as noted from Fig. 4, is large. However, the device has to be immune to disturbances prior to mass detection to ensure reliable operation. This may impose limitations on how large the amplitude of oscillation can be prior to the detection. If the amplitude is too large (so that it is close to the substrate), then a small external disturbance in the system may lead to pull-in and hence to false action. It is worthy to note from Figs. 4 and 5 that the maximum values of the response prior to the escape band, where the oscillator operates, are larger than the values of the response after the escape band. This is because of the hardening behavior characterizing clamped-clamped microbeams. It is desirable to have the opposite scenario; that is, to have the resonator operates at small amplitude prior to the escape band. This may enhance the stability of the oscillator before actuation. Moreover, it leads to a sharper transition between the unactuated and actuated states of the switch, which is a desirable feature of switches including radio-frequency (rf) switches. These reasons motivate the exploration of the STMT concept in cantilever microbeams, which is the subject of Sec. 3.

3 Primary Resonance of Cantilever Beams

Cantilever microbeams do not suffer midplane stretching, which is a cubic nonlinearity, as the case of clamped-clamped microbeams. Hence, in the presence of nonlinear electrostatic forces, which are quadratic in nature, they exhibit pure softening behavior at large deflection. This should lead to smaller amplitude prior to the escape band compared with that after the escape band. To demonstrate the idea, consider a parallel-plate capacitor employing a cantilever beam as its upper electrode. The microbeam is made of silicon with $L=100$ μm, $b=10$ μm, $h=0.1$ μm, and $d=2$ μm. The microbeam is biased by $V_{dc}=0.4$ V. The quality factor of the microbeam is assumed to be 100. The natural frequency of this microbeam $\omega_{natural}=3.3\omega_{universal}$. When the beam is biased by $V_{dc}=0.4$ V, it drops to $\omega_{natural}=3.5\omega_{universal}$. The pull-in voltage for the microbeam due to dc voltage only is $V_{dc}=0.6$ V. We begin this investigation by exploring the large-amplitude dynamics of the cantilever when excited at various harmonic frequencies. Figure 6 shows a "general map" for the response of the cantilever microbeam to an electric load of $V_{ac}=0.1$ V. The figure reveals three distinctive resonances at half (superharmonic), twice (subharmonic), and at the fundamental natural frequency (primary) of the cantilever microbeam. This complicated response is a direct consequence of the quadratic nonlinear electrostatic force. Of the three, primary and subharmonic resonances show the largest responses with very interesting characteristics. We shall discuss the primary resonance case in this section and consider the subharmonic resonance in Sec. 4.

3.1 Cantilever-Based STMT. As seen in Fig. 6, there is an apparent escape band of frequencies where the cantilever cannot be oscillating in a steady-state motion. To confirm whether this is a "must" escape band (with absolutely no possibility of a stable behavior) requires using a shooting technique, similar to Refs. [39,40]. We observe from Fig. 6 that the left branch of the frequency-response curve, before the escape band, has lower values than those after the escape band. Figure 7 illustrates utilizing this behavior to realize a STMT device of sharper transition between the on and off states of the switch. For convenience, the figure shows nondimensional plots and parameters. The figure

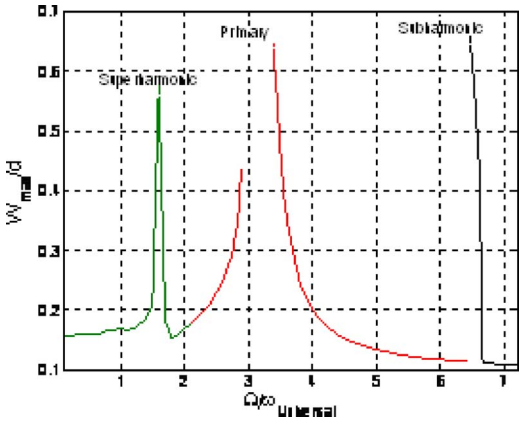

Fig. 6 Frequency response of the electrically actuated cantilever microbeams showing superharmonic, primary, and subharmonic resonances. An escape band of frequency is shown near primary resonance.

shows the microbeam oscillating steadily before mass detection at $\Omega/\omega_{universal}=2.86$. Then, by absorbing an analyte of mass equal to 3% of the beam's original mass, the ratio $\Omega/\omega_{universal}$ shifts to 2.9, where the microbeam collapses to pull-in as a switch. For $\Omega/\omega_{universal}=2.86$, the mass threshold is approximately equal to 1.5% of mass, below which the microbeam does not collapse, and beyond which the microbeam collapses. If it is desired to increase the value of the mass threshold, the initial operating point of the microbeam should be shifted further to the left away from the escape band. Thus, more mass is needed to cause the required shift of frequency to the escape band. On the other hand, if it is desired to lower this mass threshold, the initial operating frequency of the microbeam has to be selected further to the right, as close as possible to the escape band.

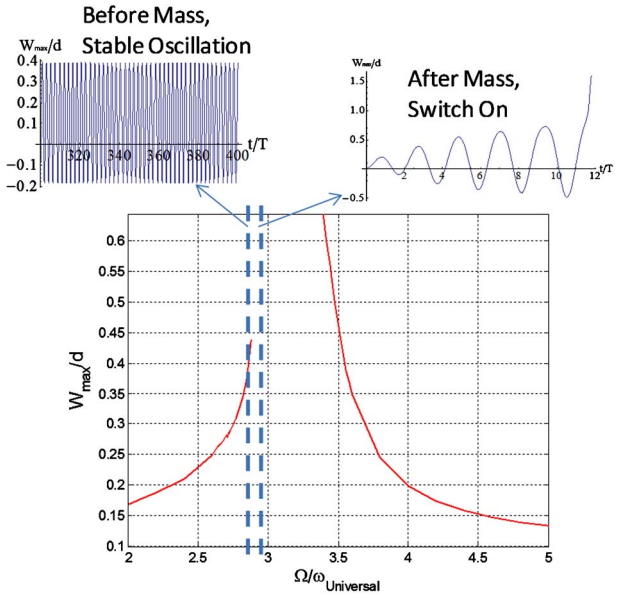

Fig. 7 Frequency response of the cantilever microbeams of Fig. 6 near primary resonance illustrating the concept of STMT. The dashed line to the left represents the operating point of the microbeam before the mass detection. The dashed line to the right represents the operating point of the microbeam after detecting an analyte, which increases its mass by 3%. The upper figures show the time history of the microbeam response before and after the mass detection. The time t is normalized to $\tilde{t}=0.04$ ms.

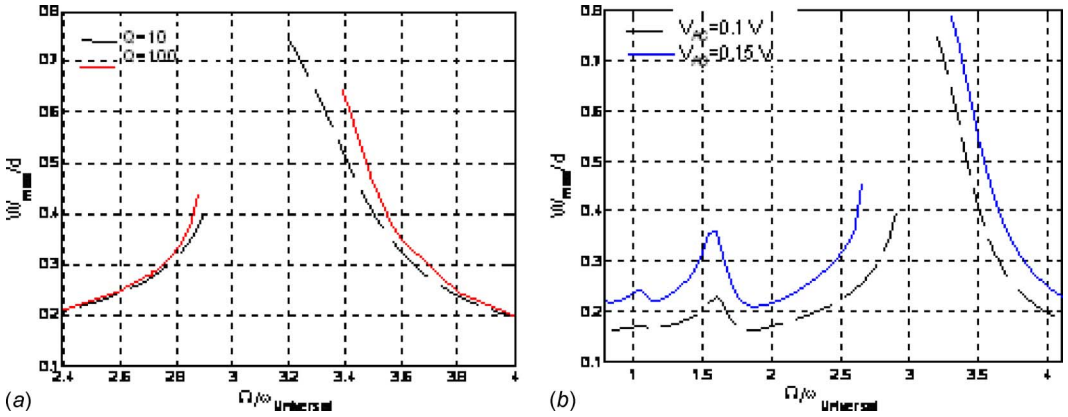

Fig. 8 Frequency-response curves for a cantilever microbeam excited at primary resonance illustrating the influence of changing the quality factor Q and ac amplitude V_{ac}. (a) V_{ac}=0.1 V, (b) Q=10.

One desirable characteristic of this switch is to have a very steep slope for the frequency-response curve before the escape band. This leads to more dramatic transition for the response from small stable amplitude motion to large unstable motion that leads to pull-in. Also, a steeper curve means more change in displacement for the same frequency shift, which means higher sensitivity. In this study, we explored the effect of damping and ac amplitude on the microbeam of Fig. 7. Figure 8(a) shows two curves of quality factors of 100 and 10. It is clear that a higher quality factor leads to steeper curves and an increased width of the escape band. Increasing the ac amplitude has a similar effect, as seen in Fig. 8(b), with stronger impact. We note that although the amplitude of the frequency-response curve before the escape band has been lowered compared with that after the escape band, it is still moderately large near 0.3–0.4. It is desirable to lower these values further. It turns out that this can be achieved using subharmonic excitation, as will be explained in Sec. 4.

3.2 Discussion. The case of primary resonance excitation of a cantilever beam actuated by electrostatic force has many similarities with the well-known problem of exciting harmonically a spring-mass-damper oscillator with quadratic stiffness nonlinearity [47]. If the mass of the oscillator is excited by a harmonic load of amplitude F and frequency Ω, then a bifurcation diagram can be established for the system to indicate all the possible scenarios for its dynamical response including the escape phenomenon. Figure 9 shows a schematic for this bifurcation diagram. This figure is explained in more detail in Ref. [47]. In the figure, for any point F and Ω below the dashed line there is no possibility for the escape phenomenon to take place. Above the dashed line, two scenarios may occur. If F and Ω are in the shaded gray area then the escape phenomenon occurs definitely. This case develops at a frequency close to the fundamental natural frequency of the system and at relatively large forcing amplitude. If F and Ω lie in the nonshaded area above the dashed line, the system can oscillate in a stable state. However, there is a possibility that system escapes from the potential well in this regime. This possibility increases as the operating point (F,Ω) approaches the gray shaded area. In this regime, whether escape occurs or not depends on the initial conditions of the system (fractal behavior).

The basic idea of the STMT is to have the microbeam operates close to this shaded area (instability tongue) before mass detection. Once the microbeam detects an external mass, the operating point shifts to the shaded area, causing its collapse as a switch. Figure 10 shows the calculated instability tongue, using time integration, for the cantilever microbeam for the case of Q=100 as a function of V_{ac} and $\Omega/\omega_{universal}$. As mentioned earlier, another technique, such as shooting methods [39,40], is recommended to confirm these results. Figure 10 also illustrates the STMT principle based on the V_{ac}-$\Omega/\omega_{universal}$ diagram. The initial operating point of the microbeam has to be ensured to be adequately stable against external disturbances before mass detection. Particularly, the microbeam needs to be ensured to operate in a safe basin of attraction zone away from the tongues of instability that develop

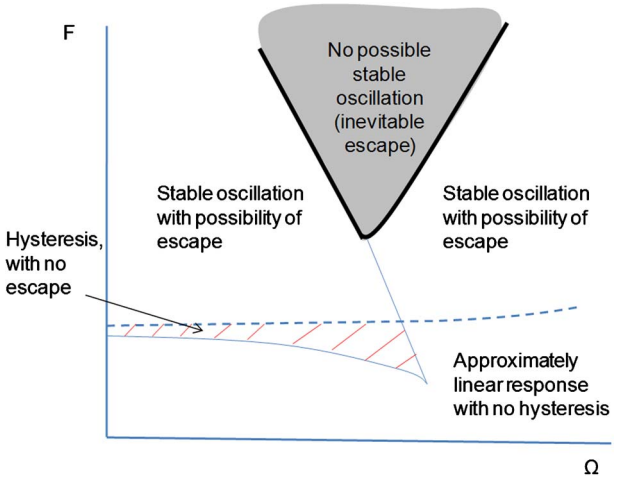

Fig. 9 Bifurcation diagram showing several scenarios for the dynamical state of a spring-mass-damper system with quadratic stiffness nonlinearity [47]

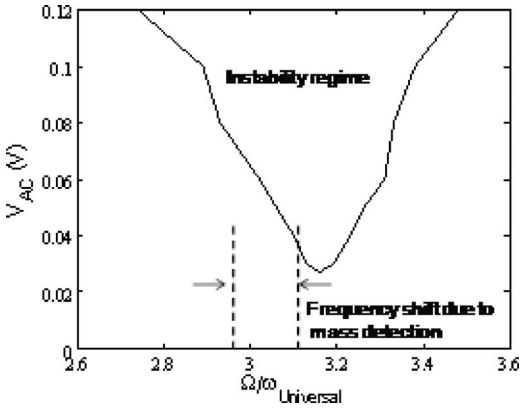

Fig. 10 The instability tongue of an electrically actuated cantilever beam illustrating the idea of the STMT based on primary resonance excitation

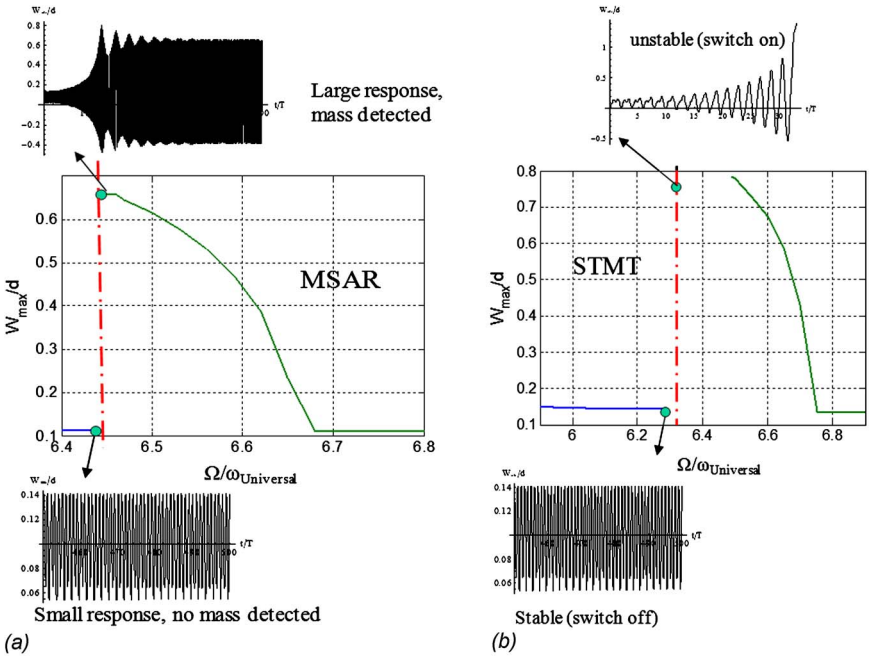

Fig. 11 The operating principle of the STMT and MSAR for the case of subharmonic resonance excitation of a cantilever microbeam. The microbeam is biased by a dc voltage equal to 0.4 V and its quality factor is equal to 100. (*a*) $V_{ac}=0.1$ V, (*b*) $V_{ac}=0.2$ V.

because of the homoclinic tangling. This requires investigating the global dynamics of the microbeam for a grid of various initial conditions, similar to the analysis in Ref. [48].

4 Subharmonic Resonance in Cantilever Beams

In this section we explore the dynamic behavior of a cantilever beam excited by subharmonic resonance of order one-half and its potential applications for mass sensing and detection. We consider the same microbeam of Sec. 3. We assume a quality factor of 100. The microbeam is biased by $V_{dc}=0.4$ V and its natural frequency is $\omega_{natural}=3.3\omega_{universal}$. By exciting the microbeam at $V_{ac}=0.1$ V with $\Omega/\omega_{universal}\approx 6.5$, subharmonic resonance is activated (Fig. 11(*a*)). The frequency-response curve in this case has very distinctive properties. Unlike the case of primary resonance, the microbeam here experiences a sudden and sharp jump from very small response to very large one as the frequency is swept passing resonance. Also, there is no multivalued solution or hysteresis once the jump occurs. This is because the small-amplitude solution loses its stability to the new born large-amplitude solution through a pitchfork bifurcation [46].

4.1 Mass Sensor of Amplified Response . Based on the interesting behavior of Fig. 11(*a*), we propose a second kind of mass sensor, which we will dub mass sensor of amplified response (MSAR). The idea of this mass sensor is to have the microbeam oscillates at the flat regime of the frequency-resonance curve (before the activation of the subharmonic resonance). Once the beam absorbs mass (can be very small amount), $\Omega/\omega_{universal}$ shifts to the right and jumps to a significantly larger amplitude. This sudden change in the microbeam response/deflection can be used as an indication of mass detection. The new and large response of the microbeam can be calibrated to the amount of detected mass. The deflection of the microbeam can be monitored using an optical read out system, similar to that used in atomic force microscopes (AFMs) or other static-mode sensors that measure beam deflection due to bending stress [49]. Figure 11(*a*) illustrates the principle of operation of this sensor. The figure compares between the time-history response for the microbeam before and after mass detection. As noted from the figure, if the microbeam is made to oscillate on the flat regime just before the escape band, a very sensitive mass sensor can be realized. This mass sensor belongs to the class of mass sensors, which monitor the change in amplitude of oscillation rather than the change in frequency shift [1]. It has the advantage of generating a strong signal that is easily measured when detecting an analyte.

An important advantage in operating the microbeam at twice its natural frequency at subharmonic resonance is the fact that the frequency shift due to the picked-up mass is being doubled compared with the conventional primary resonance mode. This means doubling the sensitivity of mass sensing. This is true for the MSAR and also for the conventional cantilever mass and gas sensors that rely on frequency shifts. For example, in the previous case, the natural frequency of the microbeam is $3.3\omega_{universal}$ and subharmonic resonance is activated at approximately twice that near $2\times 3.3\omega_{universal}$. If the microbeam picks up some mass Δm, its natural frequency decreases to $3.3\times(\omega_{universal}-\Delta\omega_{universal})$, where $\Delta\omega_{universal}=\sqrt{Ebh^3/12\Delta mL^3}$. Subharmonic resonance in this case will be activated at $2\times 3.3(\omega_{universal}-\Delta\omega_{universal})$. So the total shift in frequency in subharmonic resonance is $2\times 3.3\Delta\omega_{universal}$, which is twice that of primary resonance $(3.3\Delta\omega_{universal})$.

4.2 A Sensitive STMT. By increasing V_{ac} further to $V_{ac}=0.2$ V, dynamic pull-in and the escape phenomenon occur (Fig. 11(*b*)). This can be utilized to realize a STMT with improved sensitivity and sharpness of response. The microbeam can be made to oscillate just before the escape band with very small amplitude. Once a small amount of analyte is detected, $\Omega/\omega_{universal}$ shifts to the right and the beam collapses to transmit an electrical signal (switch is on). As can be noted here, the jump in the response of the microbeam before and after mass detection is very dramatic. The amplitude of motion before the escape band is much smaller than that of any of the previous cases of primary resonance excitation.

Next, we demonstrate by simulation the sensitivity of the STMT to detect small mass. We assume the cantilever beam ex-

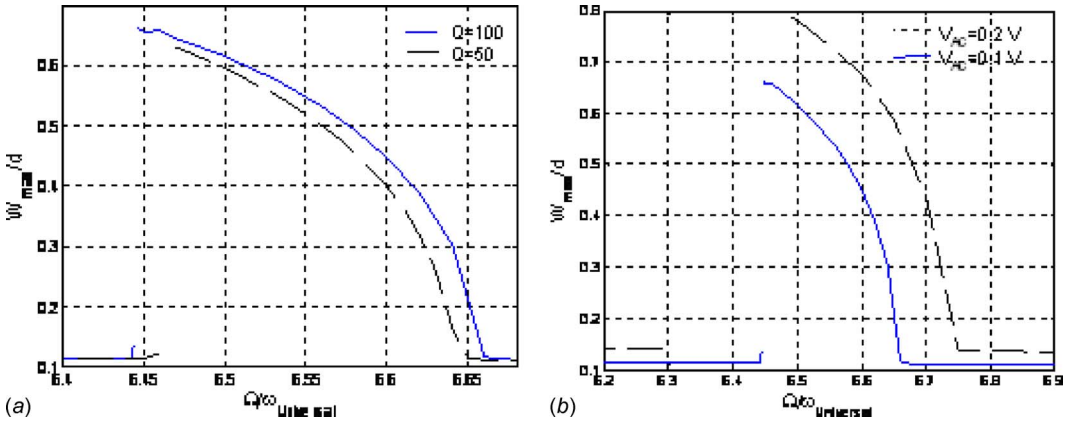

Fig. 12 Frequency-response curves for a cantilever microbeam excited at subharmonic resonance illustrating the influence of the quality factor Q and ac amplitude V_{ac}. (a) $V_{ac}=0.1$ V, (b) $Q=100$.

cited at $\Omega/\omega_{\text{universal}}=6.29$, which is just before the escape band. Figure 11(b) shows a time history for the response of the microbeam obtained by time integration for a long period of time. The figure shows clearly a steady-state stable oscillation. Next, we assume that the microbeam has picked up an analyte that resulted in increasing its mass by 0. 032%. The mass of the microbeam is 2.332×10^{-10} g, so the picked-up mass is approximately 7.4×10^{-14} g. The picked-up mass shifts $\Omega/\omega_{\text{universal}}$ to 6.291. Figure 11(b) shows the response of the microbeam in this case indicating unstable response leading to pull-in and hence closing a circuit as a switch.

4.3 The Activation of Subharmonic Resonance. The activation of subharmonic resonance requires the ac amplitude and the quality factor to exceed specific threshold levels [40,50]. Below these threshold levels, subharmonic resonance is not activated. For example, if the quality factor Q is reduced to 25, subharmonic resonance does not get activated. When Q is increased to 50 it is activated, see Fig. 12(a) with no escape band. Hence, this case can be utilized for MSAR. Increasing Q to 100 leads to the development of the escape band. Figure 12(b) shows that V_{ac} has relatively similar effect as Q. Exciting the microbeam at $V_{ac}=0.05$ V does not activate subharmonic resonance. Increasing V_{ac} to 0.1 V and then to 0.2 V activates subharmonic resonance and creates the escape band, respectively. The Q-V_{ac} zone of activation can be estimated numerically by running several simulations for various grid values of Q and V_{ac}. Figure 13 shows the Q-V_{ac} curve for the microbeam studied in this section. As shown in the figure, at small values of quality factor, high ac loads are required to activate subharmonic resonance. A similar conclusion was drawn for the activation of parametric resonance [32–34]. An example for subharmonic resonance activated at low value of Q and high value of V_{ac} is depicted in Fig. 14. The figure shows what it seems other bifurcations activated in the range of $\Omega/\omega_{\text{universal}}=5.58-5.7$ near the maximum deflection of the response.

5 Subharmonic Resonance of Clamped-Clamped Beams

In Sec. 4, we explored subharmonic resonance in cantilever beams and found that it leads to an interesting dynamical behavior that is promising for mass sensing application. In this section we revisit clamped-clamped beams and explore their potential advantage for mass sensing and detection based on their dynamic behavior when excited at subharmonic resonance. The dynamics of a clamped-clamped microbeam excited at subharmonic resonance have been first analyzed in Ref. [40] without emphasis in its application. Also the escape phenomenon has not been reported or explored in Ref. [40]. In this section, we extend the analysis in Ref. [40] and shed light on its practical application for mass sensing.

5.1 MSAR Based on a Clamped-Clamped Microbeam. Let us consider the same microbeam of Sec. 2 of length $L=510$ μm. The microbeam is biased by $V_{ac}=2$ V and has a quality factor equal to 100. If the microbeam is excited by $V_{ac}=0.6$ V of fre-

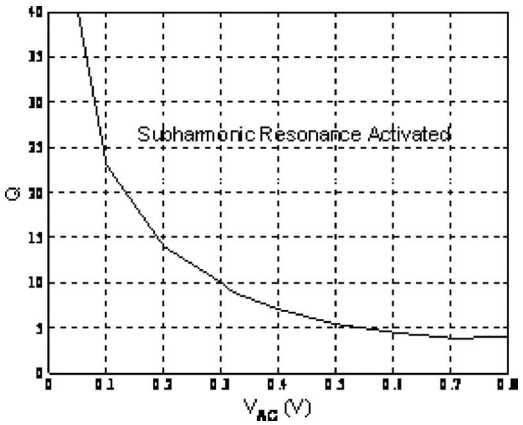

Fig. 13 The Q-V_{ac} curve showing the subharmonic resonance activation zone for a cantilever beam. For any point of Q and V_{ac} above the curve, subharmonic resonance is activated.

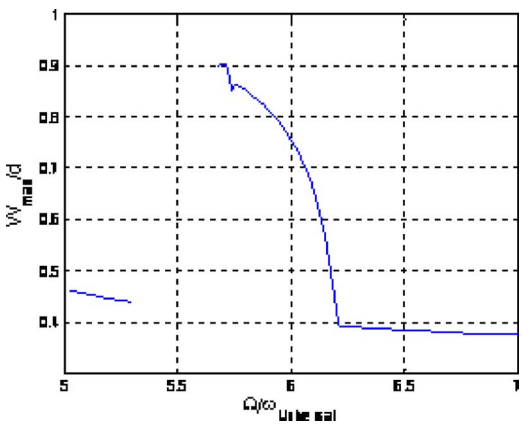

Fig. 14 Frequency-response curves for a cantilever microbeam excited at subharmonic resonance for the case of $Q=5$ and $V_{ac}=0.7$ V

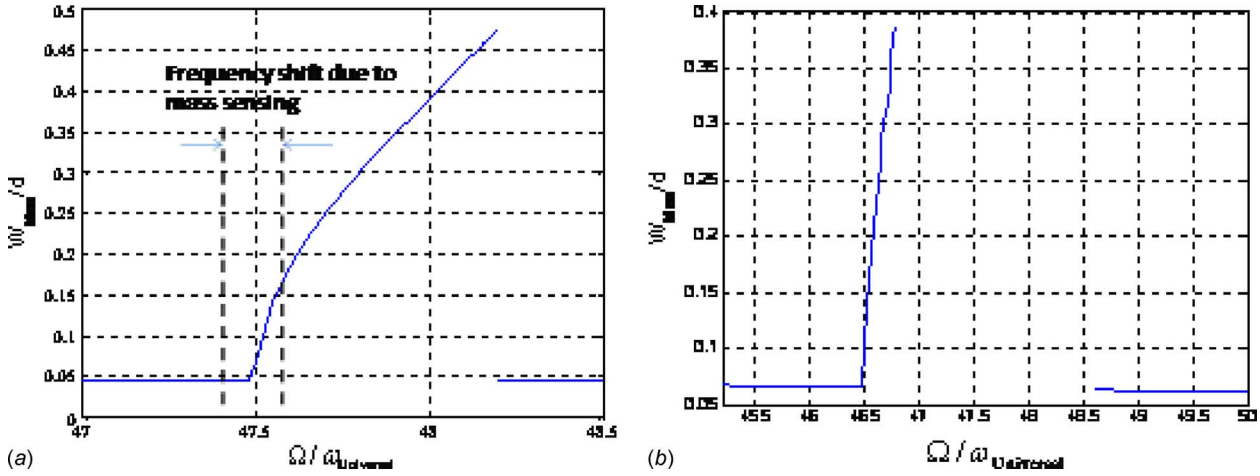

Fig. 15 Frequency-response curves showing subharmonic resonances of a clamped-clamped microbeam for various V_{ac}. (*a*) demonstrates MSAR idea based on subharmonic resonance. (*b*) indicates a wide escape band of frequencies developed at higher V_{ac}. (*a*) $V_{ac}=0.6$ V, (*b*) $V_{dc}=1.5$ V.

quency Ω near twice its natural frequency ($\Omega/\omega_{universal}\approx 48$) subharmonic resonance will be activated via a pitchfork bifurcation [40,50] (Fig. 15(*a*)). The frequency-response curve here can also be utilized to design MSAR. The differences between the properties of this mass sensor compared with that of cantilever beams, Fig. 11(*a*), are that it has wider frequency range and it is easier to be calibrated (the larger the displacement is, the larger the amount of mass detected is). However, the response here does not encounter sharp transition between the states of no-mass and with-mass states. Each of these device concepts needs further future investigation to compare between them and determine their feasibility and practicality. It is worthy to note that a similar device concept has been explored by Zhang et al. [33] using parametric excitation of a comb-drive structure with structural legs of cubic nonlinearity. The main differences between the method in Ref. [33] and the proposed method is that the proposed MSAR does not require external parametric force but requires parallel-plate electrostatic actuation to provide quadratic nonlinearity. It is worthy to note that electrostatically-actuated structures with ac harmonic excitation are intrinsically parametric [51]. Hence, they share similarities with parametrically actuated devices.

5.2 A Combined MSAR and STMT. Next, we explore another case when $V_{ac}=1.5$ V (Fig. 15(*b*)). The figure shows subharmonic resonance, which is terminated by dynamic pull-in, after which an escape band of frequencies is born. The subharmonic resonance curve is very steep making it a good candidate for mass sensing applications. Based on this interesting dynamic behavior, we propose to utilize this mechanism of actuation to realize both MSAR and STMT devices on the same microbeam at the same time. To realize a mass sensor, the microbeam needs to operate at the flat regime of the frequency-response curve, as shown in Fig. 16, for instance, at $\Omega/\omega_{universal}=46.45$ with $W_{max}/d=0.06$. If the microbeam picks or absorbs an analyte, the operating point of the microbeam will shift to the right to ride the subharmonic resonance curve, for example, at $\Omega/\omega_{universal}=46.69$ with W_{max}/d

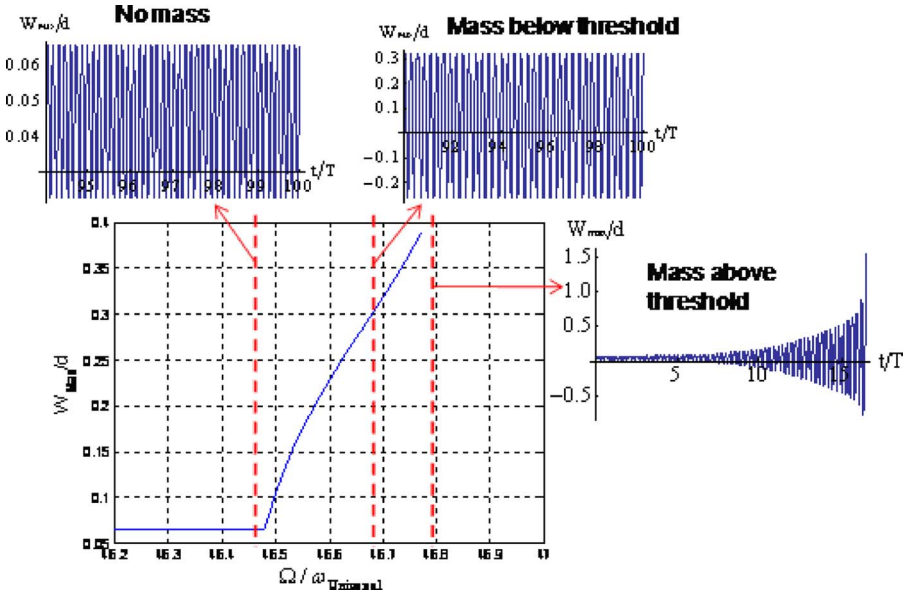

Fig. 16 Frequency-response curve and time histories of a clamped-clamped microbeam excited at subharmonic resonance illustrating its utilization for STMT and MSAR at the same time. The first dashed line to the left indicates the original operating point and the other dashed lines indicate the new operating points upon mass detection.

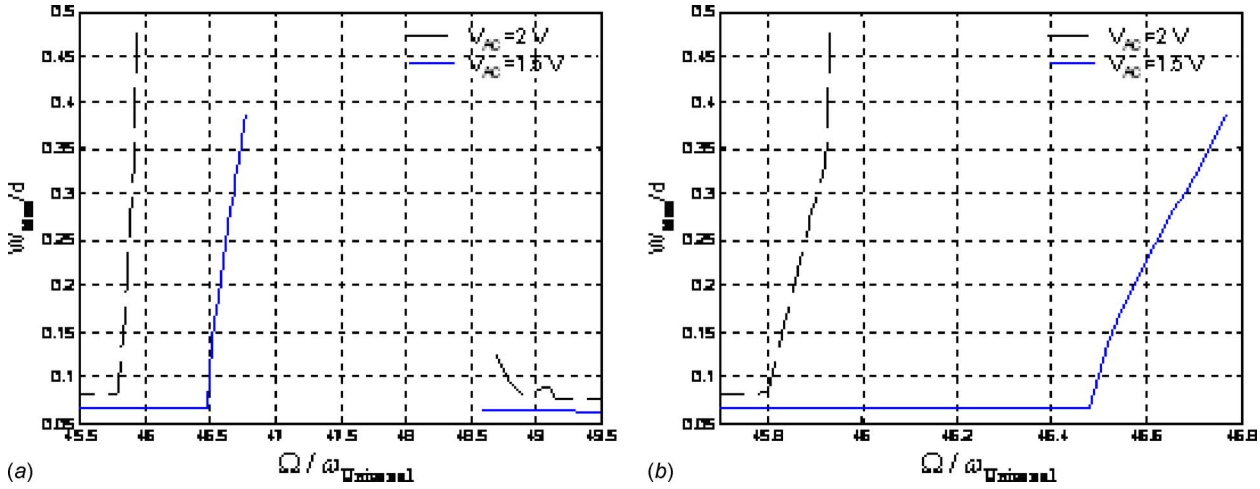

Fig. 17 (*a*) **Frequency-response curves for a clamped-clamped microbeam excited at subharmonic resonance illustrating the influence of the quality ac amplitude V_{ac}.** (*b*) **A zoomed view of** (*a*).

=0.3. This new amplified response of the microbeam can be related to the amount of mass absorbed or detected. If the amount of detected mass exceeds a specific threshold, $\Omega/\omega_{\text{universal}}$ shift to the escape band of frequencies, for example, $\Omega/\omega_{\text{universal}}=46.8$, forcing the microbeam to collapse as a switch (STMT). Such complicated functionality is desirable in some applications, where both a sensor and a switch are required. For example, the MSAR can be used to monitor the concentration of a harmful gas in the environment. However, if a certain concentration of the gas is exceeded, an immediate action is required, such as the activation of a warning system. This becomes the role of the STMT, which makes an action when exceeding a certain analyte threshold. This example demonstrates the realization of two smart sensors using the same microbeam based on the nonlinear dynamics. These types of devices can be very promising for monitoring harmful gases and substances in the environment.

By increasing the ac amplitude further, the escape band gets wider (Fig. 17(*a*)). But more importantly, the slope of the frequency-response curve prior to the escape band gets larger, as depicted in Fig. 17(*b*). The implication of this is an increased sensitivity since a larger jump in the amplitude of the response occurs for a specific frequency shift due to mass pickup. Table 1 clarifies this point further.

Figure 18 demonstrates the realization of very sensitive STMT based on this excitation method for the case of $V_{ac}=2.0$ V. If this microbeam is coated with a sorbent material and made to oscillate at $\Omega/\omega_{nat}\approx 45.9$, then by absorbing a small amount of analyte, as low as 0.18% of its mass ($\Delta m\approx 3.21\times 10^{-10}$ g), then $\Omega/\omega_{\text{universal}}$ increases to lie in the escape band of frequencies. This leads to dynamic pull-in making the switch in the "on" state.

6 Case Study

6.1 Experimental Investigation. In this section, we demonstrate experimentally some of the concepts discussed in Secs. 2–5. A capacitive accelerometer, fabricated by Sensata Technologies, Boston, MA [52], is used in this investigation (Fig. 19(*a*)). This sensor employs two cantilever beams with a proof mass at the tip of length=9 mm and width=5.32 mm. The behavior of this system is qualitatively similar to a cantilever beam excited by electrostatic force, which has been simulated earlier in this paper. The sensor is made of an alloy 42 metal of thickness 150 μm. The experimental setup used for testing, depicted in Fig. 19(*b*), is composed of a laser-Doppler vibrometer, which is used to monitor the deflection of the proof mass, a vacuum chamber, ac and dc power sources, and a LABVIEW data acquisition system.

We first tested the response of the cantilevers to a dc load only. We found the pull-in voltage for this device to be approximately 110 V, see Fig. 20. Also, we found the gap width separating the upper from lower electrode to be near 42 μm. From this static analysis of the device, and using a spring-mass model (Sec. 6.2), we estimated an effective stiffness for the system $k=215$ N/m. The next step was to measure the linear natural frequency of the system. We tested the device using small values of ac and dc loads ($V_{dc}=2$ V and $V_{ac}=4.2$ V) and found the first natural frequency to be approximately equal to 192.5 Hz. From this value and the extracted stiffness k, we estimated a value for the mass m to be used in the spring-mass model of Sec. 6.2.

The next step in the experiment was to actuate the device using large values of ac and dc loads ($V_{dc}=40.1$ V and $V_{ac}=18.4$ V) at reduced pressure (150 mtorr) to generate nonlinear responses. Figure 21 shows the frequency response for a wide range of frequency (1–400 Hz). In this figure, only the dynamic part of the proof mass deflection is shown (the static deflection due to the dc load is not shown since the laser-Doppler vibrometer cannot read it while measuring the dynamic deflection). Three distinctive resonances are depicted in the figure: superharmonic resonance of order 2, subharmonic resonance of order 1/2, and primary resonance. The figure also shows an apparent escape zone of frequencies near primary resonance, where no stable oscillation of the

Table 1 The jump in the amplitude of the response of a clamped-clamped microbeam excited at subharmonic resonance when detecting an analyte of mass equivalent to 0.5% of the beam's original mass for two ac values

V_{ac} (V)	$\Omega/\omega_{\text{universal}}$ before	$\Omega/\omega_{\text{universal}}$ after	W_{max}/d before	W_{max}/d after	$\Delta W_{max}/d$
1.5	46.48	46.596	0.0656	0.227	0.16
2.0	45.8	45.914	0.0822	0.32	0.24

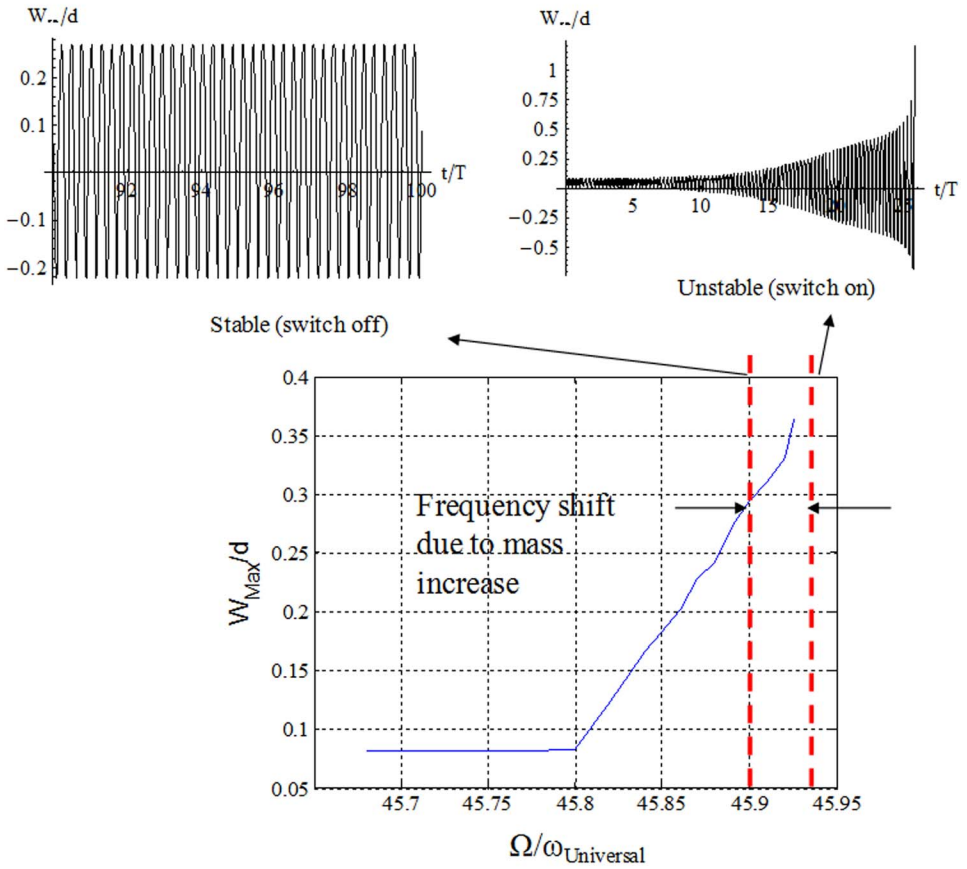

Fig. 18 The operating principle of STMT for the case of subharmonic excitation of a clamped-clamped microbeam. The dashed line to the left represents the operating point of the microbeam before the mass detection. The dashed line to the right represents the operating point of the microbeam after detecting an analyte, which increases its mass by 0.18%. The upper figures show the time history of the response before and after the mass detection. The time *t* is normalized to *T*=0.07 ms.

system can exist (escape to dynamic pull-in). One also can note that this figure shares many similarities with Fig. 6.

6.2 Modeling and Comparison With Experiment. This section presents a model for the capacitive device of Sec. 6.1. A comparison between the experimental data and the model predictions is also made. We utilize a nonlinear single-degree-of-freedom model to simulate the device response due to V_{dc} plus V_{ac} electric loading. In this model, the proof mass of the device is modeled as a lumped mass m, which forms one side of a variable capacitor. The equation of motion governing the behavior of the resonator can be written as

$$m\ddot{x} + c(x)\dot{x} + kx = \frac{\varepsilon A[V_{dc} + V_{ac}\cos(\Omega t)]^2}{2(d-x)^2} \tag{11}$$

where x is the deflection of the proof mass, Ω is the ac voltage frequency, the superscript dot denotes time derivative, A is the

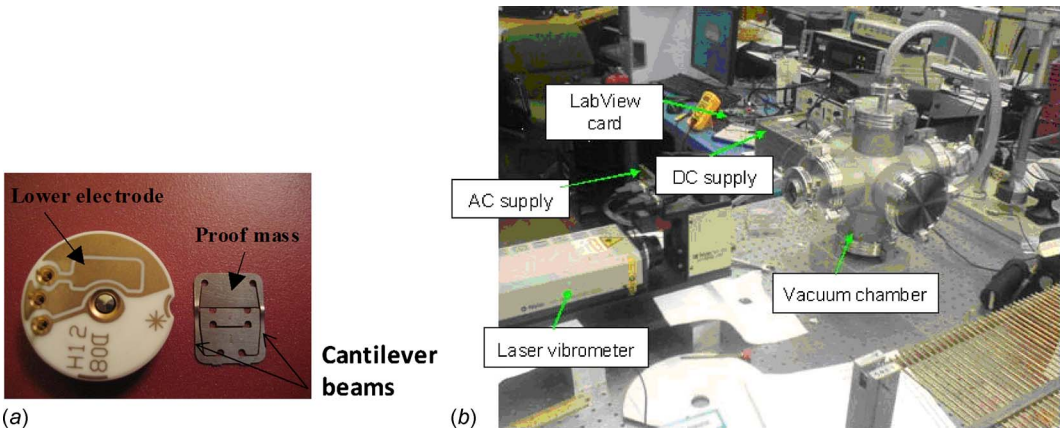

Fig. 19 (*a*) A picture for the tested capacitive sensor (taken apart) and (*b*) the experimental setup used for testing the capacitive accelerometers under reduced pressure

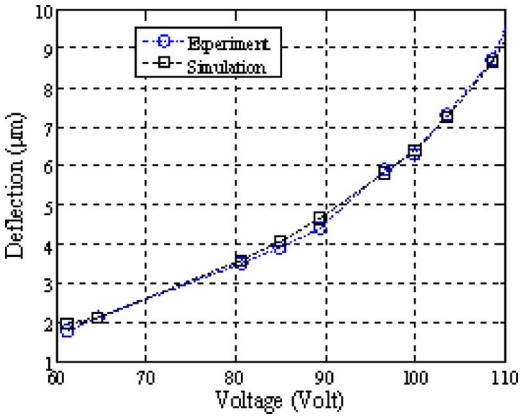

Fig. 20 The static deflection of the proof mass for different values of V_{dc}. Shown in the figure are the experimental measurements and the simulated static deflection using a spring-mass model.

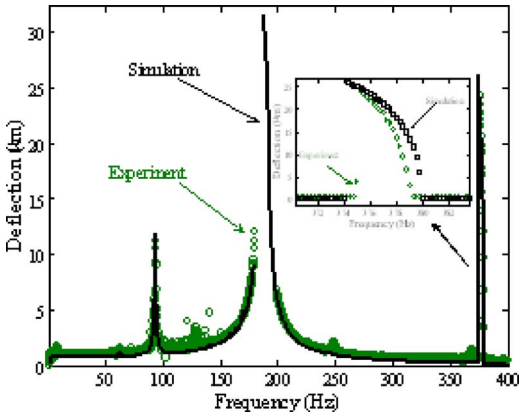

Fig. 22 Experiment (forward sweep) versus simulation results of the frequency response of the device when V_{dc}=40.1 V and V_{ac}=18.4 V.

electrode area assuming a complete overlapping between the two electrodes of the capacitor, d is the capacitor gap width, c is the squeeze-film damping coefficient, k is the effective stiffness of the cantilever beams, and ε is the dielectric constant of the gap medium. Values for k and m have been extracted, as described in Sec. 6.1. To model the squeeze-film effect, we use the Blech model [53]. The model will be modified to make the gap space varies with the proof mass motion. Therefore, c is expressed as

$$c(x) = \frac{768\,\eta_{\text{eff}} P_a A^2}{\pi^6 (d-x)^3}\left(\frac{2}{[4+\sigma^2/\pi^4]}\right)$$

where $\sigma = 12A\Omega\eta_{\text{eff}}/P_a(d-x)^2$, p_a is the ambient pressure, and η_{eff} is the effective air viscosity coefficient. Here, we truncated the series in the Blech model [53] to one term since it turns out in this studied case that using one term yields adequate accuracy and convergence. To simulate the dynamic response of the capacitive sensor, Eq. (11) is integrated numerically over time using Runge–Kutta scheme to obtain steady-state solution.

In Fig. 22 we compare the experimental frequency-response of Fig. 21 with the simulation results. The figure shows a good agreement with a slight deviation in the subharmonic resonance case. One possible reason for this is the variation in damping during the frequency sweep, which we observed during the experiment. Hence, it is hard to use a single value of pressure in the model that fits the primary and secondary resonances at the same time. In addition, we note that the experimental right stable branch of the primary resonance terminates at a very small deflection compared with theory. The reason for this is that while performing the forward frequency sweep, the system went to pull-in. We then continued the forward seep starting from an arbitrary frequency that we estimated to give a stable response and probably passing through any possible escape or pull-in frequency zone. To catch the rest of the right branch of the primary resonance, a backward frequency sweep needs to be conducted. A backward sweep for the case of primary resonance is shown in Fig. 23 with comparison with the simulation results.

To simulate the process of detecting an external mass or an analyte, small amounts of epoxy were applied to the proof mass of the capacitive sensor, Fig. 24, using a pipette. Initially, the sensor was excited near primary resonance using low values of ac and dc voltages (V_{dc}=8.0 V and V_{ac}=9.76 V) to guarantee linear response at a pressure value near 148 mtorr. The resonance frequency of the system was measured before and after the application of the added mass, see Fig. 25(*a*). The added mass causes a 0.7 Hz frequency shift in the fundamental natural frequency of its cantilever beams corresponding to an added mass equal to 1.07 μg compared with the original mass of 147 μg. Next, the sensor was driven by large values of ac and dc voltages (V_{dc} =40.1 V and V_{ac}=18.4 V) to realize dynamic pull-in and escape

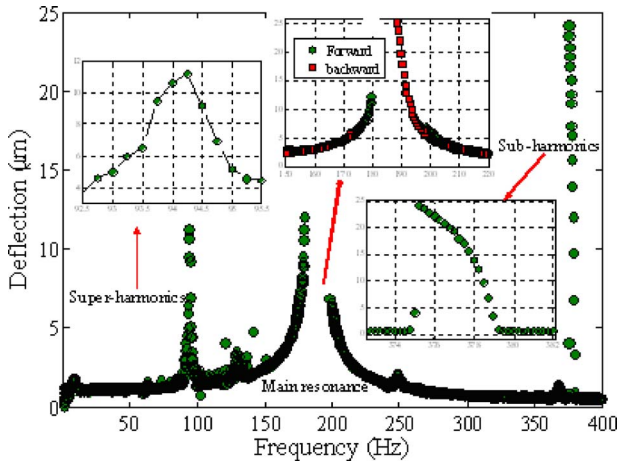

Fig. 21 A frequency sweep response for V_{dc}=40.1 V and V_{ac} =18.4 V with the pressure=150 mtorr. A sampling rate of 0.25 Hz/s was used in this experiment.

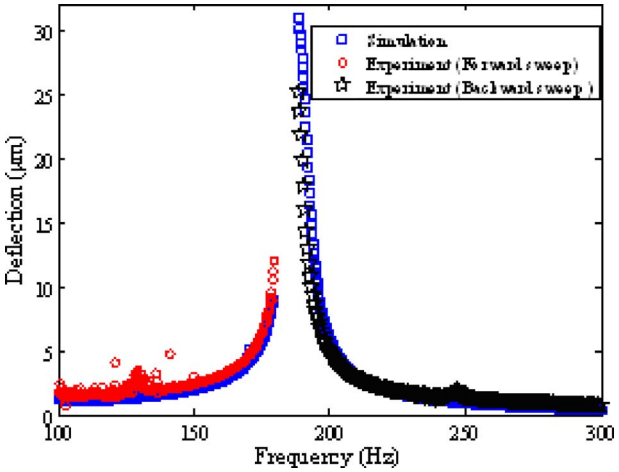

Fig. 23 Experiment (backward and forward sweeps) versus simulation results for the frequency response of the device around primary resonance

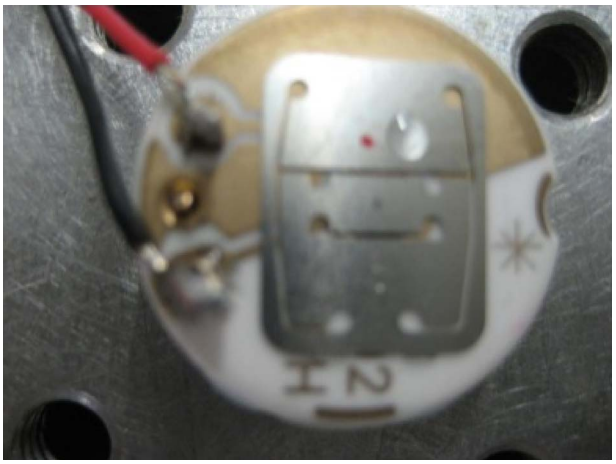

Fig. 24 A picture showing the capacitive sensor with the added mass on top of the proof mass of the device

phenomenon, which are the base of the STMT. Figure 25(*b*) shows the obtained data. The figure reveals an apparent band of frequencies where the system escapes to pull-in. Whether this is an inevitable (must) escape band of frequencies or represents a fractal behavior that leads to pull-in cannot be judged from the experimental data only. However, one can note a shift in this pull-in band due to the addition of mass. This shift is proportional to the added mass. As seen from the figure, it is difficult to realize a stable operation before the escape band of frequency, which becomes unstable after mass detection. Hence, subharmonic resonance might be of more benefit for such application.

Next, we excite the system near subharmonic resonance by applying a dc voltage equal to 40.1 V and an ac voltage equal to 18.4 V, see Fig. 26(*a*). Those voltage values were chosen carefully to avoid any escape or dynamic pull-in. Figure 26(*a*) shows clearly how the subharmonic excitation could be utilized for detecting mass change. If we consider, for example, the excitation frequency of 374 Hz in the case of the no added mass we notice that the sensor response is very small (around 0.6 μm). On the other hand, at the same excitation frequency the sensor response is very high (around 23.6 μm) for the case of the added mass. Now, with a previous calibration, this drastic change in the sensor amplitude for the same excitation frequency can be used to determine the amount of the added mass.

Increasing the ac voltage further to V_{ac}=21.1 V leads to a dynamic pull-in, see Fig. 26(*b*). The figure demonstrates how subharmonic resonance can be utilized to design a switch that is activated by mass detection. If we consider, for example, the excitation frequency of 373 Hz for the no added mass case we notice that the sensor response is very small (around 0.5 μm). On the other hand, at the same excitation frequency the sensor response is unstable and goes to pull-in when the mass is added.

These are some issues of concern for the switch idea. Among those is its stability before mass detection against external disturbances, temperature variations, excitation variations, and fabrica-

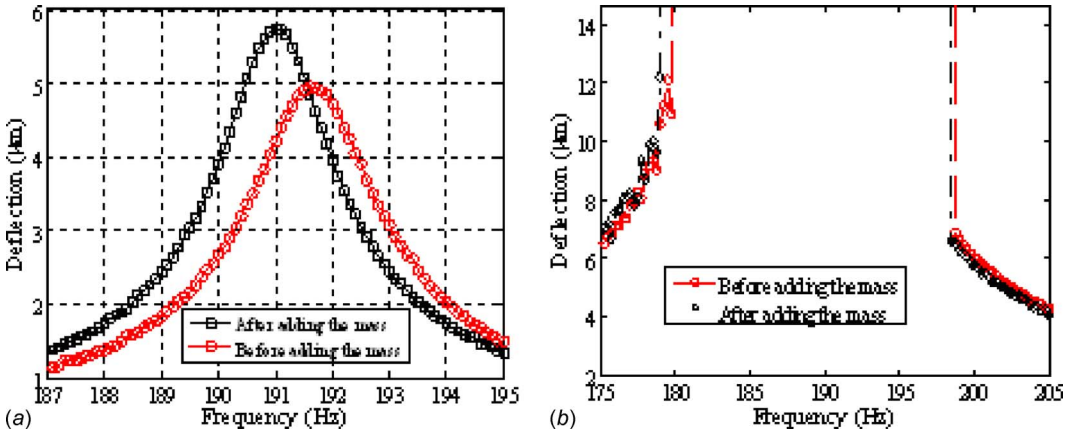

Fig. 25 The capacitive accelerometer frequency response when excited near primary resonance before and after adding the mass. (*a*) Small linear response, (*b*) large response with pull-in gap.

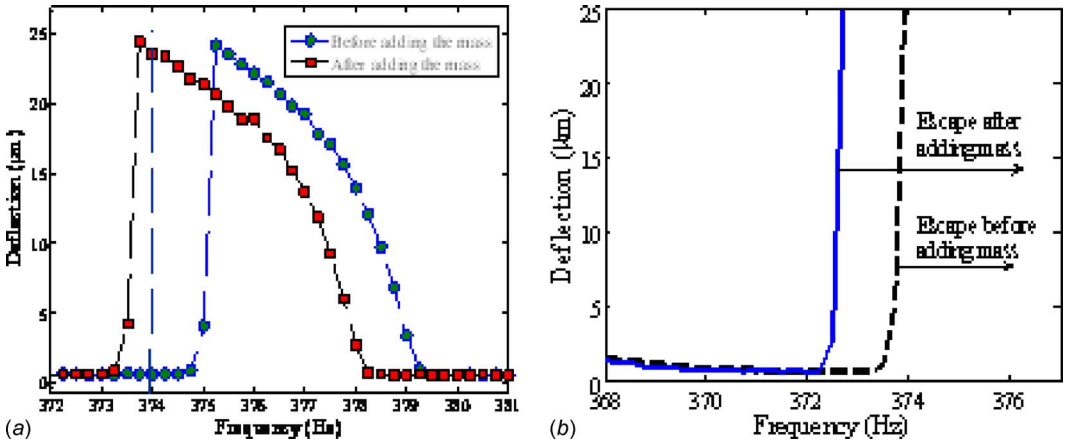

Fig. 26 The capacitive accelerometer frequency response when excited near subharmonic resonance (twice the natural frequency) before and after adding the mass. (*a*) Small response, (*b*) large response.

tion tolerances. Also, its sensitivity to thermal and electrical noise is of concern. These issues and how to control them need further investigation in the future.

7 Summary and Conclusions

This study presented exploratory research into the utilization of the escape-from-a-potential-well and jump phenomena in electrostatically-actuated resonators to realize new concepts for mass sensing and detection. These concepts rely on actuating a structure by a dc load superimposed to an ac harmonic load of frequency near its fundamental natural frequency or its twice. This frequency of actuation is kept fixed throughout the mass detection process. Hence, these mass detectors do not require phase-locked controllers to track the resonance frequency of the structure. Both clamped-clamped and cantilever microbeams were studied by simulations as case studies under various excitation methods. An experimental case study for a captive sensor employing cantilever beams was also presented demonstrating the proposed concepts. It is concluded that subharmonic excitation for either beam at twice their natural frequencies provides the most attractive features. It provides sharp transition from the no-mass to the detected-mass states and it is slightly influenced by damping changes. However, it may not get activated in high damping conditions, which put some limitations on its use.

One explored idea of a device is the STMT. This concept can be useful in applications where measuring the quantity of detected mass is not as important as doing an action upon detection. This may suit applications, such as detecting explosives, hazardous and poisonous gases, and dangerous viruses and bacteria, such as anthrax. The proposed switch idea can benefit such applications by providing an electrical signal that can be functionalized directly to a useful action without the need to complicated circuitry, controllers, and decision units. Hence, it can be made of attractively low cost. The reliability of this device, its performance under thermal variations and other disturbances, and its re-usability after switching (postswitching scenarios including stiction problems) are all issues that need future investigation.

The second kind of proposed devices is a MSAR. This sensor utilizes the change in amplitude of oscillation, rather than frequency shift, to indicate the quantity of mass being measured. Because of the pitchfork bifurcation encountered in this device concept, the amplitude change is sharp and significant. This enables precise measurements of the amplitude change using a readout mechanism, such as capacitive, piezoelectric, or optical. Another advantage of this sensor is that it also does not require a feedback or phase-locked controller to track resonance. However, a disadvantage of the sensor is that its output is not digital as the classical sensors, which produce frequency shifts. Which category of sensors is more advantageous and how they are compared against each other need further research. Also, the aforementioned issues for STMT apply for the MSAR and need be investigated.

In conclusion, it is worthy to mention that the proposed concepts of devices discussed in this paper need to be investigated for their sensitivity to external disturbances, fabrication tolerances, and noises. An important issue is the fact that those devices are based on having a resonator operating in a stable state at a fixed frequency prior to mass detection. Hence, the stability of operation prior to mass detection must be ensured to prevent accidental or erroneous switching due to disturbances or noises. This can be investigated by conducting global dynamic analysis to track the basin of attraction of the stable solution before the escape band of frequency or before the activation of subharmonic resonance. One way to improve the stability of the STMT is to have the resonator operates away from the pull-in/escape regime. However, this comes on the expense of the sensitivity of the switch, i.e., it takes larger amount of mass to have the switch triggered when it is operated initially away from the escape instability. To resolve these issues, active control strategies need to be implemented to ensure adequate stability before mass detection.

References

[1] Lange, D., Brand, O., and Baltes, H., 2002, *CMOS Cantilever Sensor Systems: Atomic-Force Microscopy and Gas Sensing Applications*, Springer, Berlin.

[2] Lange, D., Hagleitner, C., Hierlemann, A., Brand, O., and Baltes, H., 2002, "Complementary Metal Oxide Semiconductor Cantilever Arrays on a Single Chip: Mass-Sensitive Detection of Volatile Organic Compounds," Anal. Chem., **74**, pp. 3084–3095.

[3] Betts, T. A., Tipple, C. A., Sepaniak, M. J., and Datskos, P. G., 2000, "Selectivity of Chemical Sensors Based on Micro-Cantilevers Coated With Thin Polymer Films," Anal. Chim. Acta, **422**, pp. 89–99.

[4] Battiston, F. M., Ramseyer, J. P., Lang, H. P., Baller, M. K., Gerber, C., Gimzewski, J. K., Meyer, E., and Güntherodt, H. J., 2001, "A Chemical Sensor Based on a Microfabricated Cantilever Array With Simultaneous Resonance-Frequency and Bending Read-Out," Sens. Actuators B, **77**, pp. 122–131.

[5] Thundat, T., Wachter, E. A., Sharp, S. L., and Warmack, R. J., 1995, "Detection of Mercury Vapor Using Resonating Micro-Cantilevers," Appl. Phys. Lett., **66**, pp. 1695–1697.

[6] Dufour, I., Lochon, F., Heinrich, S., Josse, F., and Rebière, D., 2007, "Effect of Coating Viscoelasticity on Quality Factor and Limit of Detection of Microcantilever Chemical Sensors," IEEE Sens. J., **7**(2), pp. 230–236.

[7] Lang, H. P., Berger, R., Battiston, F., Ramseyer, J. P., Meyer, E., Andreoli, C., Brugger, J., Vettiger, P., Despont, M., Mezzacasa, T., Scandella, L., Guentherodt, H. J., Gerber, C., and Gimzewski, J. K., 1998, "A Chemical Sensor Based on a Micromechanical Cantilever Array for the Identification of Gases and Vapors," Appl. Phys. A: Mater. Sci. Process., **66**, pp. S61–S64.

[8] Lochon, F., Fadel, L., Dufour, I., Rebiere, D., and Pistre, J., 2006, "Silicon Made Resonant Microcantilever: Dependence of the Chemical Sensing Performances on the Sensitive Coating Thickness," Mater. Sci. Eng., C, **26**(2–3), pp. 348–353.

[9] Fadel, L., Lochon, F., Dufour, I., and Francais, O., 2004, "Chemical Sensing: Millimeter Size Resonant Microcantilever Performance," J. Micromech. Microeng., **14**, pp. S23–S30.

[10] Spletzer, M., Wu, Q., Raman, A., Xu, X., and Reifenberger, R., 2006, "Ultrasensitive Mass Detection Using Mode Localization in Coupled Microcantilevers," Appl. Phys. Lett., **88**, p. 254102.

[11] Burg, T. P., Mirza, A. R., Milovic, N., Tsau, C. H., Popescu, G. A., Foster, J. S., and Manalis, S. R., 2006, "Vacuum-Packaged Suspended Microchannel Resonant Mass Sensor for Biomolecular Detection," J. Microelectromech. Syst., **15**(6), pp. 1466–1476.

[12] Raiteri, R., Grattarola, M., Butt, H., and Skladal, P., 2001, "Micromechanical Cantilever-Based Biosensors," Sens. Actuators B, **79**, pp. 115–126.

[13] Ilic, B., Czaplewski, D., Zalalutdinov, M., Craighead, H. G., Neuzil, P., Campagnolo, C., and Batt, C., 2001, "Single Cell Detection With Micromechanical Oscillators," J. Vac. Sci. Technol. B, **19**, pp. 2825–2828.

[14] Gupta, A., Akin, D., and Bashir, R., 2004, "Single Virus Particle Mass Detection Using Microresonators With Nanoscale Thickness," Appl. Phys. Lett., **84**, pp. 1976–1978.

[15] Lavrik, N. V., Sepaniak, M. J., and Datskos, P. G., 2004, "Cantilever Transducers as a Platform for Chemical and Biology Sensors," Rev. Sci. Instrum., **75**, pp. 2229–2253.

[16] Ono, T., Li, X. X., Miyashita, H., and Esashi, M., 2003, "Mass Sensing of Adsorbed Molecules in Sub-Picogram Sample With Ultrathin Silicon Resonator," Rev. Sci. Instrum., **74**, pp. 1240–1243.

[17] Ekinci, K. L., Huang, X. M. H., and Roukes, M. L., 2004, "Ultrasensitive Nanoelectromechanical Mass Detection," Appl. Phys. Lett., **84**, pp. 4469–4471.

[18] Forsen, E., Abadal, G., Ghatnekar-Nilsson, S., Teva, J., Verd, J., Sandberg, R., Svendsen, W., Perez-Murano, F., Esteve, J., Figueras, E., Campabadal, F., Montelius, L., Barniol, N., and Boisen, A., 2005, "Ultrasensitive Mass Sensor Fully Integrated With Complementary Metal Oxide Semiconductor Circuitry," Appl. Phys. Lett., **87**, p. 043507.

[19] Vancura, C., Rüegg, M., Li, Y., Lange, D., Hagleitner, C., Brand, O., Hierlemann, A., and Baltes, H., 2003, "Magnetically Actuated CMOS Resonant Cantilever Gas Sensor for Volatile Organic Compounds," IEEE 12th International Conference on Solid State Sensors and Actuators, Vol. 2, pp. 1355–1358.

[20] Ekinci, K. L., Yang, Y. T., and Roukes, M. L., 2004, "Ultimate Limits to Inertial Mass Sensing Based Upon Nanoelectromechanical Systems," J. Appl. Phys., **95**, pp. 2682–2689.

[21] Yang, J., Ono, T., and Esashi, M., 2000, "Mechanical Behavior of Ultrathin Microcantilever," Sens. Actuators, A, **82**, pp. 102–107.

[22] Lavrik, N. V., and Datskos, P. G., 2003, "Femtogram Mass Detection Using Photothermally Actuated Nanomechanical Resonators," Appl. Phys. Lett., **82**, pp. 2697–2699.

[23] Ilic, B., Craighead, H. G., Krylov, S., Senaratne, W., Ober, C., and Neuzil, P., 2004, "Attogram Detection Using Nanoelectromechanical Oscillators," J. Appl. Phys., **95**, pp. 3694–3703.

[24] Jin, D., Li, X., Liu, J., Zuo, G., Wang, Y., Liu, M., and Yu, H., 2006, "High-Mode Resonant Piezoresistive Cantilever Sensors for Tens-Femtogram Resoluble Mass Sensing in Air," J. Micromech. Microeng., **16**(5), pp. 1017–1023.

[25] Tseytlin, Y. M., 2005, "High Resonant Mass Sensor Evaluation: An Effective Method," Rev. Sci. Instrum., **76**, p. 115101.

[26] Dohn, S., Sandberg, R., Svendsen, W., and Boisen, A., 2005, *Enhanced Functionality of Cantilever Based Mass Sensors Using Higher Modes*, American Institute of Physics, New York, Vol. 86.

[27] Dohn, S., Sandberg, R., Svendsen, W., and Boisen, A., 2005, "Enhanced Functionality of Cantilever Based Mass Sensors Using Higher Modes and Func-

tionalized Particles," International Conference on Solid State Sensors and Actuators and Microsystems, TRANSDUCERS '05, Vol. 2, pp. 636–639.
[28] Lochon, F., Dufour, I., and Rebière, D., 2005, "An Alternative Solution to Improve Sensitivity of Resonant Microcantilever Chemical Sensors: Comparison Between Using High-Order Modes and Reducing Dimensions," Sens. Actuators B, **108**(1–2), pp. 979–985.
[29] Chen, G., Thundat, T., Wachter, E., and Warmack, R., 1995, "Adsorption-Induced Surface Stress and Its Effects on Resonance Frequency of Microcantilevers," J. Appl. Phys., **77**, pp. 3618–3622.
[30] Li, Y., Ho, M., Hung, S., Chen, M., and Lu, C., 2006, "CMOS Micromachined Capacitive Cantilevers for Mass Sensing," J. Micromech. Microeng., **16**(12), pp. 2659–2665.
[31] Voiculescu, I., Zaghloul, M., McGill, R., Houser, E., and Fedder, G., 2005, "Electrostatically Actuated Resonant Microcantilever Beam in CMOS Technology for the Detection of Chemical Weapons," IEEE Sens. J., **5**(4), pp. 641–647.
[32] Zhang, W., and Turner, K. L., 2005, "Application of Parametric Resonance Amplification in a Single-Crystal Silicon Micro-Oscillator Based Mass Sensor," Sens. Actuators, A, **122**, pp. 23–30.
[33] Zhang, W., Baskaran, R., and Turner, K. L., 2002, "Effect of Cubic Nonlinearity on Auto-Parametrically Amplified Resonant MEMS Mass Sensor," Sens. Actuators, A, **102**(1–2), pp. 39–150.
[34] Zhang, W., and Turner, K. L., 2004, "A Mass Sensor Based on Parametric Resonance," A Solid State Sensor, Actuator and Microsystems Workshop, Hilton Head Island, SC, p. 49.
[35] Vyas, A., Bajaj, A. K., and Peroulis, D., 2007, "Nonlinear Resonator With Interacting Flexural-Torsional Modes for Mass Sensing," *Proceedings of the 21st Biennial Conference on Mechanical Vibration and Noise (VIB)*, Las Vegas, NV, Paper No. DETC2007-35117.
[36] Mehta, A., Cherian, S., Hedden, D., and Thundat, T., 2001, "Manipulation and Controlled Amplification of Brownian Motion of Microcantilever Sensors," Appl. Phys. Lett., **78**, pp. 1637–1639.
[37] Senturia, S. D., 2001, *Microsystem Design*, Kluwer Academic, Boston.
[38] Rebeiz, G. M., 2003, *RF MEMS: Theory, Design, and Technology*, Wiley, New York.
[39] Nayfeh, A. H., Younis, M. I., and Abdel-Rahman, E. M., 2007, "Dynamic Pull-In Phenomenon in MEMS Resonators," Nonlinear Dyn., **48**, pp. 153–163.
[40] Nayfeh, A. H., and Younis, M. I., 2005, "Dynamics of MEMS Resonators Under Superharmonic and Subharmonic Excitations," J. Micromech. Microeng., **15**, pp. 1840–1847.
[41] Younis, M. I., Abdel-Rahman, E. M., and Nayfeh, A. H., 2003, "A Reduced-Order Model for Electrically Actuated Microbeam-Based MEMS," J. Microelectromech. Syst., **12**, pp. 672–680.
[42] Nayfeh, A. H., Younis, M. I., and Abdel-Rahman, E. M., 2005, "Reduced-Order Models for MEMS Applications," Nonlinear Dyn., **41**, pp. 211–236.
[43] www.wolfram.com.
[44] Inman, D. J., 2001, *Engineering Vibrations*, Pearson, Upper Saddle River, NJ.
[45] Meirovitch, L., 2001, *Fundamentals of Vibrations*, McGraw-Hill, Boston.
[46] Nayfeh, A. H., and Balachandran, B., 1995, *Applied Nonlinear Dynamics*, Wiley, New York.
[47] Thompson, J. M. T., and Stewart, H. B., 2001, *Nonlinear Dynamics and Chaos*, Wiley, New York.
[48] Lenci, S., and Rega, G., 2006, "Control of Pull-In Dynamics in a Nonlinear Thermoelastic Electrically Actuated Microbeam," J. Micromech. Microeng., **16**, pp. 390–401.
[49] Lim, S., Raorane, D., Satyanarayana, S., and Majumdar, A., 2006, "Nano-Chemo-Mechanical Sensor Array Platform for High-Throughput Chemical Analysis," Sens. Actuators B, **119**, pp. 466–474.
[50] Nayfeh, A. H., 1981, *Introduction to Perturbation Techniques*, Wiley, New York.
[51] Younis, M. I., and Nayfeh, A. H., 2003, "A Study of the Nonlinear Response of a Resonant Microbeam to an Electric Actuation," Nonlinear Dyn., **31**, pp. 91–117.
[52] www.sensata.com.
[53] Blech, J. J., 1983, "On Isothermal Squeeze Films," ASME J. Lubr. Technol., **105**, pp. 615–620.